The temperature dependence of the deformation behavior of the polycrystalline silver nanowires studied by molecular dynamics simulation

Jianwei Zhao[1*], Xiuxiu Wang[2] , Gang Yu[2] , Colm Durkan[3], Nan Wang[3]

[1] College of Material and Textile Engineering, Jiaxing University, Jiaxing City, Zhejiang 314001, P. R. China

[2] College of Chemistry and Chemical Engineering, Hunan University, Changsha City, Hunan 410082, P. R. China

[3] The Nanoscience Centre, University of Cambridge, Cambridge CB3 0FF, UK

Abstract

Based on molecular dynamics simulations, the plastic deformation of columnar polycrystalline silver nanowires under uniaxial tension at different temperatures has been studied systematically. At a temperature lower than 200 K, the system with large grains deforms predominantly via the mechanism of dislocation slip, and the maximum yield strength remains relatively constant with temperature. When the simulation temperature is higher than 200 K, grain sliding gradually becomes the dominant deformation mechanism, especially for those samples with reduced grain size and the maximum yield strength shows a decrease with the increase of temperature. The temperature-dependence of the Hall-Petch relation has been discussed.

Keywords: Polycrystalline; Nanowires; Temperature; Tensile; Hall-Petch relation; Molecular dynamics

1. Introduction:

The nature and distribution of grain boundaries in polycrystalline metals plays a prominent role in determining many material properties such as interface mobility, corrosion, crack nucleation resistance, ductility, as well as the electrical and thermal transport properties[1-3]. During the past decade, tremendous efforts have been made towards improving our understanding of the atomic arrangement and mechanical behavior of polycrystalline metals by computer simulations[4-9] and careful experiments[10-17]. So far, the deformation mechanisms[18] experienced under stress conditions have been explained in terms of grain boundary (GB) sliding[19, 20], migration[21], rotation[22], and diffusion creep[23].

The GB strengthening (or Hall-Petch strengthening) [24] is a method of strengthening materials by changing their average crystallite (grain) size. It is based on the observation that grain boundaries impede the dislocation movement and that the number of dislocations within a grain have an effect on how easily dislocations can traverse grain boundaries and travel from grain to grain. Therefore, by changing the grain size one can control the dislocation movement and modulate the yield strength[25]. Experimental observations on many nanocrystalline materials have demonstrated that when the grains are of a small enough size, typically of the order 10 nm, the yield strength either remains constant or decreases with further reduction of the grain size. This phenomenon has been termed the reverse Hall-Petch relation. The Hall-Petch relation at a constant temperature has been studied intensively. Keller *et al.*[26] performed simulation of Ni polycrystals, and their results showed a deviation from the Hall-Petch formulation for samples with less than a critical number of grains in thickness. Godon *et al.*[27] reported that the size-dependence of the flow stress can be accurately described by the Hall-Petch relationship over a large range of grain sizes (d>20nm) and the Hall-Petch slope k is dependent on the orientation texture of grain boundaries. Chokshi *et al*.[28] observed the enhancement of the diffusional creep along the grain boundaries that is similar to the GB sliding, and correlated this observation with the reverse Hall-Petch relation.

In the Hall-Petch and reverse Hall-Petch relations, both dislocation slip and GB sliding are sensitive to temperature, albeit at different rates. Therefore, by changing the temperature of the system, one can modulate the deformation mechanism of the nano-sized system and further explore the material strengthening under the elevated temperature. Such an approach can ultimately be used to design materials with desired properties not only at the atomic, but also at the nanometer scale – taking into account the microstructure . In this work, we have designed polycrystalline silver nanowire samples with different length-diameter ratios and performed molecular dynamics (MD) simulations under different temperatures. The temperature dependence of the Hall-Petch relation has been discussed qualitatively.

2. Simulation method

Cuboid samples with dimensions of 15.13×15.13×29.85 nm^3 and ~0.38 million atoms were constructed using a Voronoi tessellation construction as a matrix, as shown in Figure 1. The models of columnar polycrystalline silver samples containing two grains across their width and a number of grains along their length with a random crystallographic orientation are denoted as Para2-8, Para2-12, Para2-16, Para2-20 and Para2-24. The average crystallite (grain) sizes are 11.77, 10.29, 9.34, 8.68 and 8.16 nm, respectively. MD simulations were performed on the polycrystalline structures with different length-diameter ratios using a self-developed software NanoMD[29-32]. A constant strain rate of 8.1×10^8 s^{-1} was used in all simulations (Explain why this rate was chosen). The embedded atom method (EAM) potential[33-35] was adopted to analyze the atomic interaction of Face Centered Cubic (FCC) silver atoms. Free boundary conditions were applied in all three spatial dimensions to model a columnar-like structure. Prior to any imposed stress, each sample was equilibrated at a constant temperature for 256 ps to relax out the unfavorable configurations in the grain boundaries. After reaching a steady-state arrangement, seven temperatures of 10, 50, 100, 150, 200, 250 and 300 K were held for those loads to extract temperature-dependent behaviors of the simulations. Table 1 shows the

crystallographic characteristics of all models. It shows that the proportion of grain boundary atoms increases as the number of grains increases, as expected.

The stress within the nanowire is computed by a virial scheme, and the overall stress is taken as the average of all atomistic stresses[36]. The corresponding atomic stress is expressed in terms of EAM potential functions as follows:

$$\sigma_{\alpha}^{zz} = \frac{1}{\Omega_{\alpha}}\left\{-m_{\alpha}v_{\alpha}^{z}v_{\alpha}^{z} + \frac{1}{2}\sum_{\beta\neq\alpha}\left[\frac{\partial\phi}{\partial r_{\alpha\beta}} + \left(\frac{\partial F}{\partial\rho_{\alpha}} + \frac{\partial F}{\partial\rho_{\beta}}\right)\frac{\partial f}{\partial r_{\alpha\beta}}\right]\frac{r_{\alpha\beta}^{z}r_{\alpha\beta}^{z}}{r_{\alpha\beta}}\right\} \quad (1)$$

Where σ_{α}^{zz} is the *zz* component of the atomic stress tensor of atom α, Ω_{α} is its volume, m is the mass and v_{α}^{z} is the velocity component in the z direction of the atom α. Parameters ϕ, F, ρ and f are extracted from the EAM potential. The first and second terms on the right side of the above equation represent the thermal and atomic interactions, respectively.

In order to study the structures of plastically deformed polycrystralline nanowires in detail, different types of defects are identified by means of the centro-symmetry parameter[37]. The centro-symmetry parameter can be defined as:

$$p_i = \frac{1}{D_0^2}\sum_{j=1,6}\left|R_j + R_{j+6}\right|^2 \quad (2)$$

where R_j and R_{j+6} are the vectors corresponding to the six pairs of opposite nearest neighbours in the FCC lattice, D_0 is the nearest-neighbour distance and p_i is the centro-symmetry parameter value of atom i in the lattice. For reference, $p_i < 0.4$ corresponds to the FCC structure, especially $p_i = 0$ reflects a perfect silver lattice. $0.7 < p_i < 1.2$ stands for stacking faults, corresponding to the HCP atoms. $1.2 < p_i < 1.8$ represents for atoms halfway between HCP and the surface atoms, and $p_i > 1.8$ is equivalent to surface atoms. For convenience, $p_i > 1.2$ is regarded as other atoms for discussion in the following paragraphs.

3. Results and discussion

3.1 Potential and stress-strain relation

The atoms at the grain boundary have higher potential energy than those in the

crystalline lattice, therefore the evolution of the average potential may give insight into the structural change of the system during stretching. The average potential energy-strain relationship for the polycrystalline silver samples with a set of grain sizes at different temperatures are shown in Figure 2. In general, the potential energy curve of the samples with more grains is higher than those with less grains. However, the potential evolution still has significant difference at different temperature. At low temperature, 10 K for example as shown in Figure 2(a), the potential curve has very light fluctuations due to the low kinetic energy of the atoms. The curves can be clearly divided into two parts along the strain curve. In the initial stage (the area <1>), we observe that the potential energy increases in a parabolic form（$E=kx^2$）[38], consistent with elastic deformation. The elastic constant k has the values 5.56, 5.16, 4.48, 4.43 and 4.43 meV·nm^{-2}, respectively, with increasing the number of grains or decreasing the grain size. The decrease of the elastic constant k is attributed to the high ratio of the disordered atoms at the grain boundary. In the stage denoted as area <2>, the potential energy experiences a quick decline, then, a slow increase with slight fluctuation. This stage is usually considered to generate a number of dislocation slips in the crystalline grains. At raised temperature, 100 K for example as shown in Figure 2(b), most features of the potential curves remain. However, the elastic behavior becomes less obvious, and the potential fluctuations are more clear. When the temperature is raised over 200 K, the elastic behavior no longer exists. Figure 2(c) shows the potential curves at 250 K, a typical temperature in this region. In spite of the grain size, the parabolic increase of the potential energy no longer exists even in the initial stage, inferring a plastic deformation in whole stretching. In addition, the potential fluctuations become more profound and the potential curves are close to each other, indicating a different grain size-dependence of the deformation mechanism in this temperature region.

The stress-strain relationship may also give key information about the mechanical properties of the system at the macroscopic level. Figure 3(a), (b) and (c) show the tensile stress-strain relationships of five typical samples at 10, 100 and 250 K, respectively. The tensile stress increases linearly with strain up to a certain peak stress

and then decreases steadily for all grain sizes considered in this study. The linear dependence indicates elastic behavior. The yield stress and yield strain are useful parameters to help identify the deformation mechanisms. Although the yield behavior shows some dispersivity among the samples, we can still observe general trends in the data. The yield stress decreases as the grain number increases. For example, it is decreased by 18.2% and 16.7% at 10 and 100 K respectively, when comparing Para2-8 with Para2-24. However, the yield strain does not show significant changes over a large temperature range. This result indicates that the systems investigated in this work fall into the reverse Hall-Petch regime. In order to give a definite conclusion, we have performed 5 simulations under each condition and performed a statistical analysis of the the yield stress, the yield strain and the Young's modulus as shown in Figures 3(d), 3(e) and 3(f), respectively.

In Figure 3(d), we can clearly see that the evolution of the yield stress vs. Temperature can be divided into two stages. Below 200 K, the yield stress declines slightly with increasing temperature. When the temperature is higher than 200 K, the yield stress decreases dramatically for all samples. The existence of a critical temperature indicates a different deformation mechanism that dominates the grain size-dependence of the mechanical properties. However, the yield strain has only a weak temperature dependence as shown in Figure 3(e), although it does show a small increase above 200 K. The Young's modulus is obtained from the ratio of stress to strain, therefore, it appears to have the similar behavior to the yield stress as yield strain keeps constant. From Figure 3(f) we can observe that when the temperature is reduced below 200 K, the Young's modulus decreases with a rate of 75 $MPa \cdot K^{-1}$. When the temperature is raised above this critical value, the Young's modulus decreases at a much faster rate of 250 $MPa \cdot K^{-1}$. The Young's modulus is directly correlated to the material strength. In the present study, the grain size is smaller than the Hall-Petch limit, i.e., in the reverse Hall-Petch regime. Therefore, grain boundary sliding is considered to be dominant mechanism at low temperature. However, the raised temperature provides the atoms with more kinetic energy, allowing more dislocations to be generated together with the grain boundary sliding.

3.2 The radial distribution function and the quantitative change of specific atoms

The radial distribution function (RDF) and the quantitative change of the specific atoms are important parameters bridging the macroscopic properties and the microscopic structure. Figure 4 shows the RDF features of the polycrystalline silver nanowires at the yield point. Figure 4(a) compares the RDF as a function of grain size at a typical temperature of 50 K. With decreasing the grain number, the short-range order corresponding to r *(define r)* less than 1.5 lattice spacings remains unchanged, but the long-range order corresponding to r larger than 2.5 lattice spacings decreases perceptibly. In order to elucidate the temperature-dependence of the crystalline structure, Figure 4(b) compiles the RDF curves of sample Para2-8 at different temperatures. In general, the RDF curve becomes smoother at a raised temperature, indicating that the crystalline structure is disordered by the thermal motion of atoms. To study the effects of temperature on both the short- and long-range order, we concentrate on the regions with the atomic distance between 0.6 and 0.8 (short-range order corresponding to the nearest neighbor) and between 3.0 to 4.0 (corresponding to long-range order), as shown in Figure 4(c) and 4(d), respectively. In Figure 4(c), the well-defined Gaussian peaks show the temperature-dependence. However, the RDF peak unevenly decreases with temperature. In particular, it drops by 35% as the temperature increases from 50 to 150 K, but only 14% from 200 to 300 K. Another interesting feature is displayed by the long-range order as shown in Figure 4(d). Below 200 K, the RDF peak shows a decrease with increasing temperature. However, above this temperature, the peak shifts toward large atomic distance together with slight decrease of the peak height, indicating expansion of the material. From the variation of the crystalline structure, we can identify the critical temperature, below which the crystalline order is simply decreased, and above which more complex structure distortion takes place.

Figure 5 illustrates the quantitative change of the specific atoms identified with centro-symmetry parameter during tensile loading. The centro-symmetry parameter is a useful measure of the local lattice disorder around an atom and can be used to

characterize whether the atom is part of a perfect lattice, a local defect (e.g. a dislocation or stacking fault), or at a surface. The number is calculated by subtracting the initial number (what number?) before deformation from the measured number (what number?). The change of the number of specific atoms starts after relaxation. In particular, the number of FCC atoms decreases accompanied with increase in HCP atoms. The other atoms do not show clear changes. Figures 5(a) and 5(b) show similar variations for the samples Para2-8 and Para2-12 in which the grain aspect ratios[38] are greater than 1 and can be viewed as the same group. In these two figures, only three typical temperatures are presented. At 10 and 150 K, the HCP atoms do not have obvious changes below a strain of 0.02. Above this, the number tends to increase. At the yield point as indicated by the vertical line, the increase trend becomes obvious. On the contrary, a different behaviour can be found for the sample at 250 K. Soon after the relaxation, the number of HCP atoms increase. After a small peak, the HCP atoms decrease and keep constant for a short strain region. Above a strain of 0.02, the HCP atoms restart to raise as those at low temperature. This observation implies that a number of dislocations are generated by the raised temperature but a recrystallization takes place at the beginning of stretching. Figures 5(c) and 5(d) show the evolution of the samples Para2-20 and Para2-24 in which the grain aspect ratios are less than 1. Although more grains are included in the samples, the variation of the number of the specific atoms does not show obvious difference at low temperatures as compared with the other two samples. However, at 250 K, the curves are very characteristic. HCP atoms increased dramatically after relaxation. After a small peak the number of HCP atoms decline and then increase again. Comparing the four samples, the quantitative change of the specific atoms is more dramatic for the nanowires with small grains. The variation of the number of HCP atoms reflects the change of dislocation or disordered atoms. Therefore, we can infer that as the temperature increases, the grain size-dependent deformation mechanism is changed. Especially, at temperature higher than 200 K, dislocation slip is activated, and the Hall-Petch limit shifts to larger grain size.

3.3 Atomic configuration during application of tensile stress

To further understand the temperature effect on the deformation mechanism of polycrystalline silver nanowires, the evolution of the microstructures of samples Para2-8, Para2-16 and Para2-24 under 10, 150 and 250 K, respectively, have been captured and compiled together for comparison.

Sample Para2-8 has 11.77 nm mean grain size which is close to the Hall-Petch limit. Therefore, its deformation behavior at different temperature may give insight into the temperature dependence of the shift of the Hall-Petch relation. At low temperature as shown in Figure 6(a), the first dislocations emanate from the cross point between the grain boundary and surface or the junction of grain boundaries as symbolized by the letter A. It should be also noted that the disordered atoms in the grain boundary environment possess high energy, making it easier to overcome the slip barrier. Therefore, some dislocations are generated at the grain boundary upon tensile loading as marked by the circle in the snapshot. With further stretching, voids at grain boundaries marked as "B" appear in the polycrystalline silver nanowire, leading to the final break, due to the limited number of slip systems. The material shows fragile (brittle) rather than plastic behavior. At a raised temperature, the atoms at grain boundaries become more active and dislocations can be generated directly from the grain boundary as also indicated by the letter "A" in Figure 6(b). In addition, when the leading partial dislocations reach a grain boundary, pile-ups were formed, shown by the solid circles in Figure 6. As the deformation progresses, such pile-ups serve as new dislocation nucleation sources, generating further dislocations. The atoms at grain boundary has higher energy than the bulk atoms, therefore, they may induce recrystallization as well as 图错了。. . At 250 K, most dislocations move along grain boundaries and below 5% strain, there are few dislocations in grains. Above a strain of 5%, a large number of dislocations began to move inside the grains. These results demonstrate that higher temperatures provide greater thermal energy to atoms that may generate more dislocations in the crystalline grains.

For the model Para2-16 with smaller grains, the temperature dependence of the deformation mechanism become different to that with large grains. Due to the

presence of larger numbers of grains, the dislocations have a higher probability to be generated at the grain boundary even at low temperature. As shown by the second picture in Figure 7(a), two dislocations appear with one at the surface and the other at the grain boundary. At 4.25% strain, the grain boundary appears to absorb the dislocation, and then becomes wider. With further stretching, a large number of dislocations are generated at both the surface and the grain boundaries. When the system experiences heat-treatment at 250 K for 256 ps, the crystalline atoms close to the grain boundaries tend to be melted and the grain boundaries become wider as compared to those at lower temperature. In addition, a few dislocations appear even though no stretching takes place. Figure 7(c) shows these features, demonstrating the essential change of the crystalline structure at high temperature. There features are also reflected from the quantitative change of specific atoms as given in Figure 5. The number of HCP atoms increases even after relaxation at 250 K. It is worth noting that the initial structures are changed, in other words, the nanowire is softened and the yield stress decreases significantly with further increasing temperature when the temperature is higher than 200 K (shown in Figure 3(d)). This can be understood qualitatively in that a great number of metal atoms can gain sufficient energy to overcome the activation energy barrier and rearrange the initial configuration easily at higher temperature[39]. We also observed that the first dislocations are all emitted from grain boundaries. Thereafter these dislocations migrate into grains and annihilate in grain boundaries (circles region in Figure 7).

The tensile deformation process of Ag nanowires with 24 grains is shown in Figure 8. The sample has much more grains than others, the ratio of the atoms at grain boundary is increased to 10.19%. Since more active atoms contribute to the generation of dislocations, the first dislocations are rather likely generated from grain boundaries in all temperature regimes. However, due to the small grain size, the dislocations can traverse only short distances and are blocked by either the free surface or the grain boundary. At 10 K, the material presents fragile feature that a large number of dislocations are generated in those grains located at the middle part of the nanowire. This concentration of dislocations results in the rapid necking and final

breaking. At 100 K, the dislocations generated look to be randomly populated over the whole nanowire. It should be noted that in these small grains, the dislocations generated in one grain are also difficult to traverse to the neighboring grain. However, the grain boundary is an important source for new dislocations. This might be the reason why the system with smaller grains may have lower yield stress and Young's modulus in the reverse Hall-Petch regime. Further increasing temperature may result in more melted atoms at the grain boundary. This increase of the disordered atoms is profound for the system with small grain size as also indicated by the variation of HCP atoms in Figure 5(c) and (d). High temperature improves the nanowire ductility, accompanying a number of dislocations generated even at the beginning of the stretching. However, this feature significantly decreases the system strength.

Summarising the above data analysis and discussion, we have collated the temperature effect on the tensile behavior of the polycrystalline silver nanowires as shown in Figure 9. The parabolic curve presents the Hall-Petch relation together with the reverse Hall-Petch relation. The top on the curve corresponds to the Hall-Petch limit, symbolizing the maximum attainable yield strength via grain boundary strengthening. At a temperature region lower than 200 K, the relation shifts toward large grain size when temperature increases. The maximum yield strength has also slight decline. When the temperature is higher than 200 K, with the temperature increasing, dislocation slip is the dominant deformation mechanism for polycrystalline nanowires, the maximum attainable yield strength via grain boundary strengthening fall sharply.

4. Conclusions

In this work, the effect of temperature on polycrystalline silver nanowires was studied using molecular dynamics analysis. It was found that for polycrystalline Ag nanowires, a larger number of disordered atoms in the grain boundary environment leads to grain boundaries possessing higher energy. The smaller the grain size, the higher the energy, but as temperature is increased, atomic thermal motion increases,

resulting in lower yield strength and reduced short- and long-range order of the atoms. In this work, the main finding is that the deformation mechanism of polycrystalline Ag nanowires changes with the increase of temperature. At low temperature (T<200 K) and large grain size, deformation tends to occur preferentially by dislocation slip to grain sliding. Due to the limited number of slip systems at low temperature, polycrystalline silver nanowires break by forming voids at grain boundaries upon tensile loading. In contrast, by raising the temperature (T>200 K), grain boundary sliding becomes the primary deformation mechanism and the strength of the nanowires decreases. The global plastic deformation is carried by both dislocations and grain boundary sliding.

Table 1. Crystallographic characteristics of Ag nanowires with different length-diameter ratios at 10K.

Number of grains	Equivalent grain size(d)/nm	Proportion of grain boundary atoms /%	k/meV·nm^{-2}
8	11.77	6.72	5.56
12	10.29	7.04	5.16
16	9.34	9.15	4.48
20	8.68	9.95	4.43
24	8.16	10.19	4.43

References

[1] D. P. Field and B. L. Adams, *Acta Metall. Mater*. 40, 1145 (1992).

[2] L. C. Lim, *Acta Metall*. 35, 1653 (1987).
[3] V. Randle, The Role of the Coincidence Site Lattice in Grain Boundary Engineering (Woodhead, London, 1996).
[4] H. Van Swygenhoven, *Science* 296, 66 (2002).
[5] H. Van Swygenhoven, Nature Mater. 5, 841 (2006).
[6] H. Van Swygenhoven, D. Farkas, and A. Caro, *Phys. Rev. B* 62, 831 (2000).
[7] V. Yamakov, D. Wolf, S. R. Phillpot, A. K. Mukherjee, and H. Gleiter, *Nature Mater*. 1, 45 (2002).
[8] Y. H. Wen, Z. Z. Zhu, and R. Z. Zhu, Comput. *Mater. Sci*. 41, 553 (2008).
[9] T. Zhu, J. Li, A. Samanta, H. G. Kim, and S. Suresh, *Proc. Natl. Acad. Sci. U.S.A*. 104, 3031 (2007).
[10] E. Ma, Y. M. Wang, Q. H. Lu, M. L. Sui, L. Lu, and K. Lu, *Appl. Phys. Lett*. 85, 4932 (2004).
[11] P. G. Sanders, J. A. Eastman, and J. R. Weertman, *Acta Mater*. 45, 4019 (1997).
[12] F. Sato, A. S. Moreira, J. Bettini, P. Z. Coura, S. O. Dantas, D. Ugarte, and D. S. Galvao, *Phys. Rev. B* 74, 193401 (2006).
[13] X. L. Wu and E. Ma, *Appl. Phys. Lett*. 88, 231911 (2006).
[14] D. Wang, J. Zhao, S. Hu, X. Yin, S. Liang, Y. Liu, and S. Deng, *Nano Lett*. 7, 1208 (2007).
[15] L. Lu, M. L. Sui, and K. Lu, *Science* 287, 1463 (2000).
[16] L. Lu, Y. F. Shen, X. H. Chen, L. H. Qian, and K. Lu, *Science* 304, 422 (2004).
[17] M. W. Chen, E. Ma, K. J. Hemker, H. W. Sheng, Y. M. Wang, and X. M. Cheng, *Science* 300, 1275 (2003).
[18] K. S. Kumar, H. Van Swygenhoven, and S. Suresh, *Acta Metall*. 51, 5743 (2003).
[19] J. Schiotz and K. W. Jacobsen, *Science* 301, 1357 (2003).
[20] F. Zhang, Z. Liu, and J. Q. Zhou, *Materials Letters*. 183, 261-164 (2016).
[21] H. Zhang, D. J. Srolovitz, J. F. Douglas, and J. A. Warren, *Phys. Rev. B* 74, 115404 (2006).
[22] Z. W. Shan, E. A. Stach, J. M. K. Wiezorek, J. A. Knapp, D. M. Follstaedt, and S. X. Mao, *Science* 305, 654 (2004).
[23] V. Yamakov, D. Wolf, and S. R. Phillpot, *Nature Mater*. 3, 43 (2004).
[24] H. Conrad, and J. Narayan, *Scripta Mater*. 42 (11), 1025–30 (2000).
[25] H. Conrad, and K. Jung, *Materials Science and Engineering A-Structural Materials Properties Microstrcture and Processing*. 406, 78-85 (2015).
[26] K. Clement, and H. Eric, *Materials Letters*. 62, 1718-1720 (2008).
[27] A. Godon, J. Creus, S. Cohendoz, E. Conforto, X. Feaugas, P. Girault, and C. Savall, *Scripta Materialia*. 62: 403-406 (2010).
[28] A. H. Chokshi, A. Rosen, J. Karch, and H. Gleiter, *Scripta Metallurgica*. 23(10), 1679-1683 (1989).
[29] J. W. Zhao, X. Yin, S. Liang, Y. H. Liu, D. X. Wang, S. Y. Deng, and J. Hou, *Chem. Res. Chin. Univ*. 24, 367 (2008).
[30] Y. L. Sun, Y. J. Gao, Q. Sun, and J. W. Zhao, *Acta Phys. Chim. Sin*. 31(10), 1880-1887 (2015).
[31] Y. J. Gao, Y. L. Sun, Y. B. Yang, Q. Sun, and J. W. Zhao, *Molecular Simulation*. 41(18), 1546-1552 (2015).
[32] Y. L. Sun, Y. J. Gao, W. Sun, and J. W. Zhao, *Molecular Simulation*. 41(15), 1245-1253 (2015).
[33] Y. Mishin, D. Farkas, M. Mehl, D. Papaconstantopoulos, *Phys. Rev. B* 59 (5) (1999) 3393.
[34] R. A. Johnson, *Phys. Rev. B* 37, 3924 (1988).
[35] R. A. Johnson, *Phys. Rev. B* 37, 6121 (1988).
[36] H. A. Wu, Eur. J. Mech. *A/Solids* 25, 370 (2006).
[37] Landau, L.D.; *Lifshitz, E. M*. (1986)
[38] H. A. Wu, *Eur J Mech A-Solid* 25(2), 370-377 (2006).
[39] Y. Zhao, Z. Chen, J. Long, and T. Yang, *Acta Metallurgica Sinica*. 27(1), 81-86 (2014).

Figure Captions

Figure 1. Initial configuration of Ag nanocrystalline wire with columnar grains

Figure 2. The potential energy curves for Ag nanowires at (a) 10, (b) 100, and (c) 250 K.

Figure 3. Stress-strain curves of Ag nanowires at (a) 10K; (b) 100K; (c) 250K; (d) yield stress-temperature curves; (e) yield strain-temperature curves; (f) young's modulus-temperature curves.

Figure 4. Radial distribution functions of Ag nanowires at the yield point. (a) with different length-diameter ratios at 50K; (b) the Para2-8 at different temperature; (c) enlarge the first neighbor peak in Figure (b); (d) enlarge the areas between 3 and 4 in Figure (b).

Figure 5. The reduced number of different atoms versus strain. (a) Para2-8; (b) Para2-12; (c) Para2-20; (d) Para2-24.

Figure 6. Tensile yielding of Para2-8 at (a) 10K; (b) 150K; (c) 250K.

Figure 7. Tensile yielding of Para2-16 at (a) 10K; (b) 150K; (c) 250K.

Figure 8. Tensile yielding of Para2-24 at (a) 10K; (b) 150K; (c) 250K.

Figure 9. Hall-Petch Strengthening is limited by the different temperature.

Figure 1

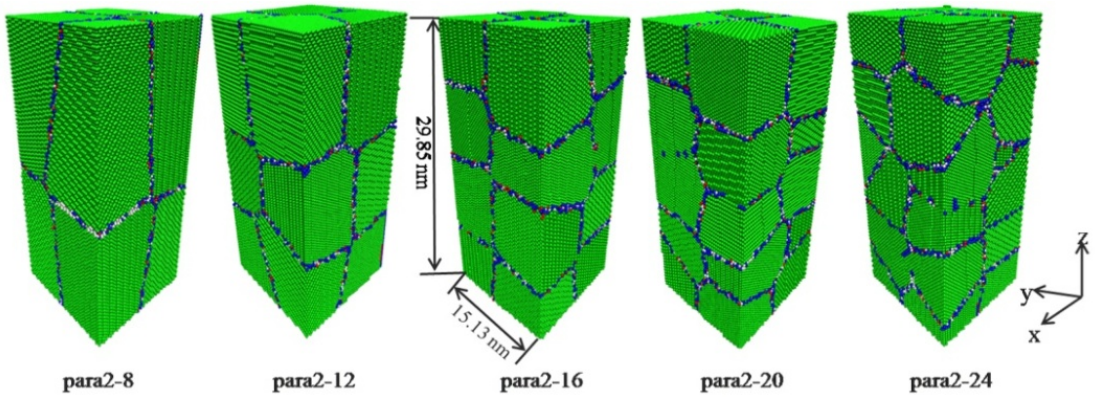

Figure 2

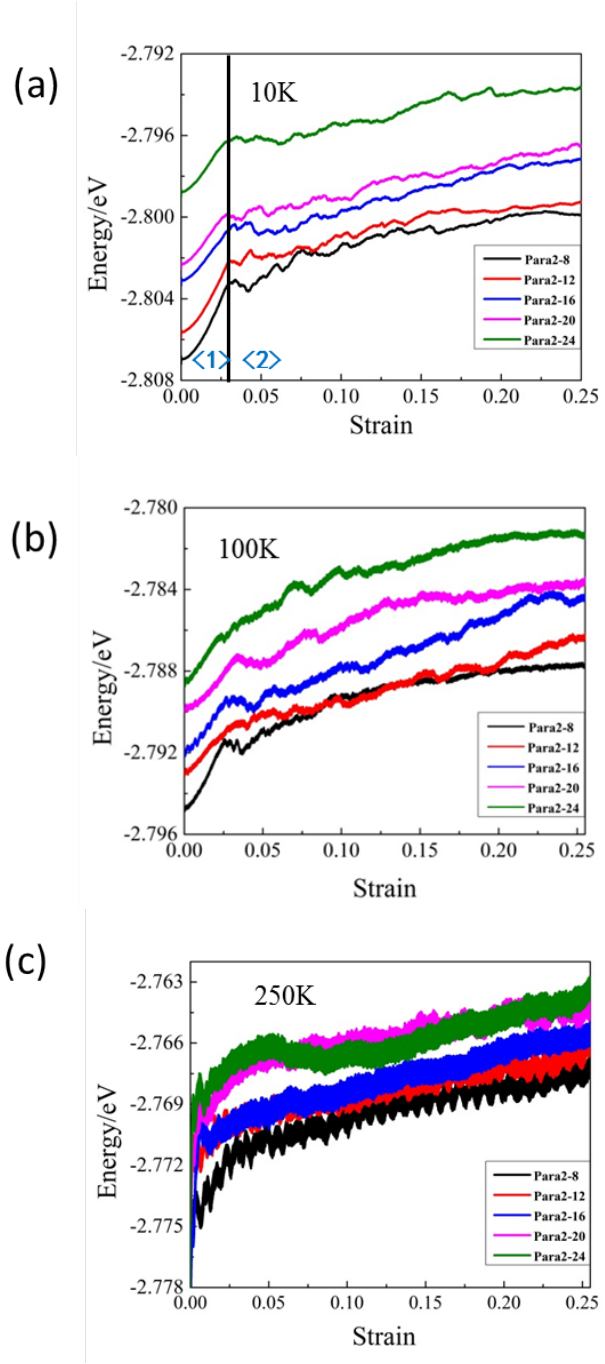
(a)
10K
Energy/eV
Strain
Para2-8
Para2-12
Para2-16
Para2-20
Para2-24
<1>
<2>
(b)
100K
Energy/eV
Strain
(c)
250K
Energy/eV
Strain

Figure 3

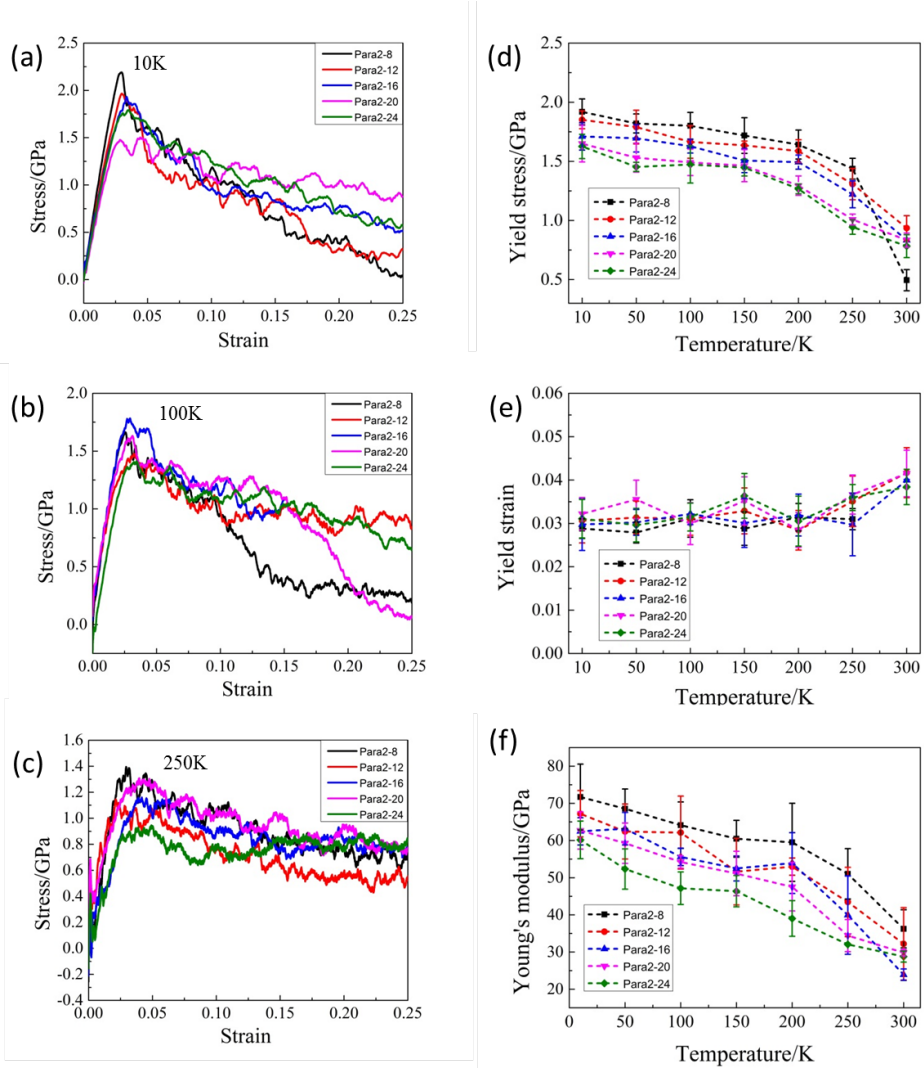
(a)
10K
Stress/GPa
Strain
(b)
100K
Stress/GPa
Strain
(c)
250K
Stress/GPa
Strain
(d)
Yield stress/GPa
Temperature/K
(e)
Yield strain
Temperature/K
(f)
Young's modulus/GPa
Temperature/K
Para2-8
Para2-12
Para2-16
Para2-20
Para2-24

Figure 4

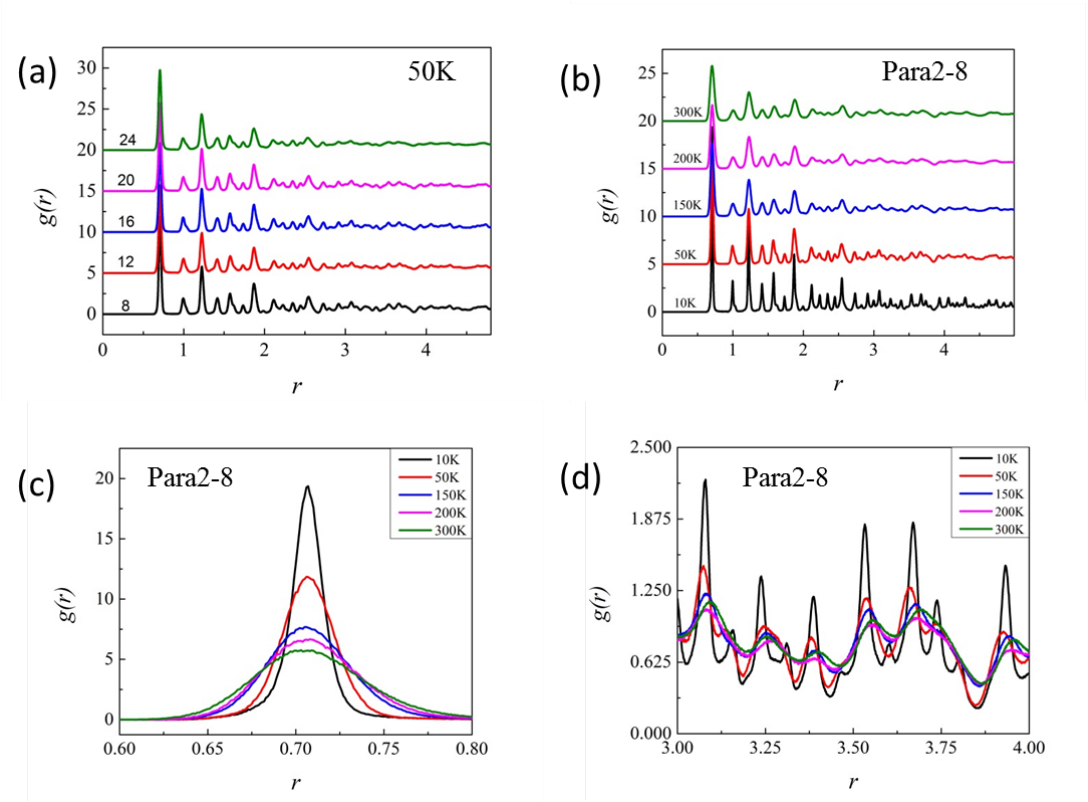
(a)
50K
24
20
16
12
8
g(r)
r
(b)
Para2-8
300K
200K
150K
50K
10K
g(r)
r
(c)
Para2-8
10K
50K
150K
200K
300K
g(r)
r
(d)
Para2-8
10K
50K
150K
200K
300K
g(r)
r

Figure 5

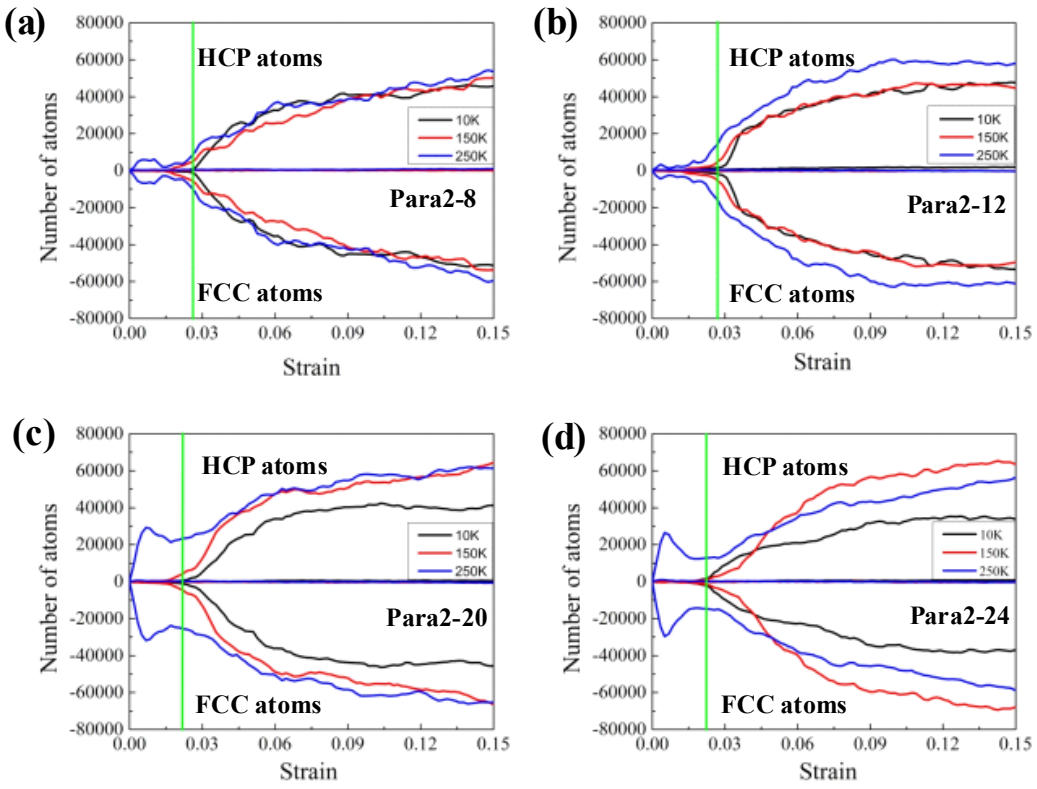
(a)
HCP atoms
Para2-8
FCC atoms
10K
150K
250K
Number of atoms
Strain
(b)
HCP atoms
Para2-12
FCC atoms
10K
150K
250K
Number of atoms
Strain
(c)
HCP atoms
Para2-20
FCC atoms
10K
150K
250K
Number of atoms
Strain
(d)
HCP atoms
Para2-24
FCC atoms
10K
150K
250K
Number of atoms
Strain

Figure 6

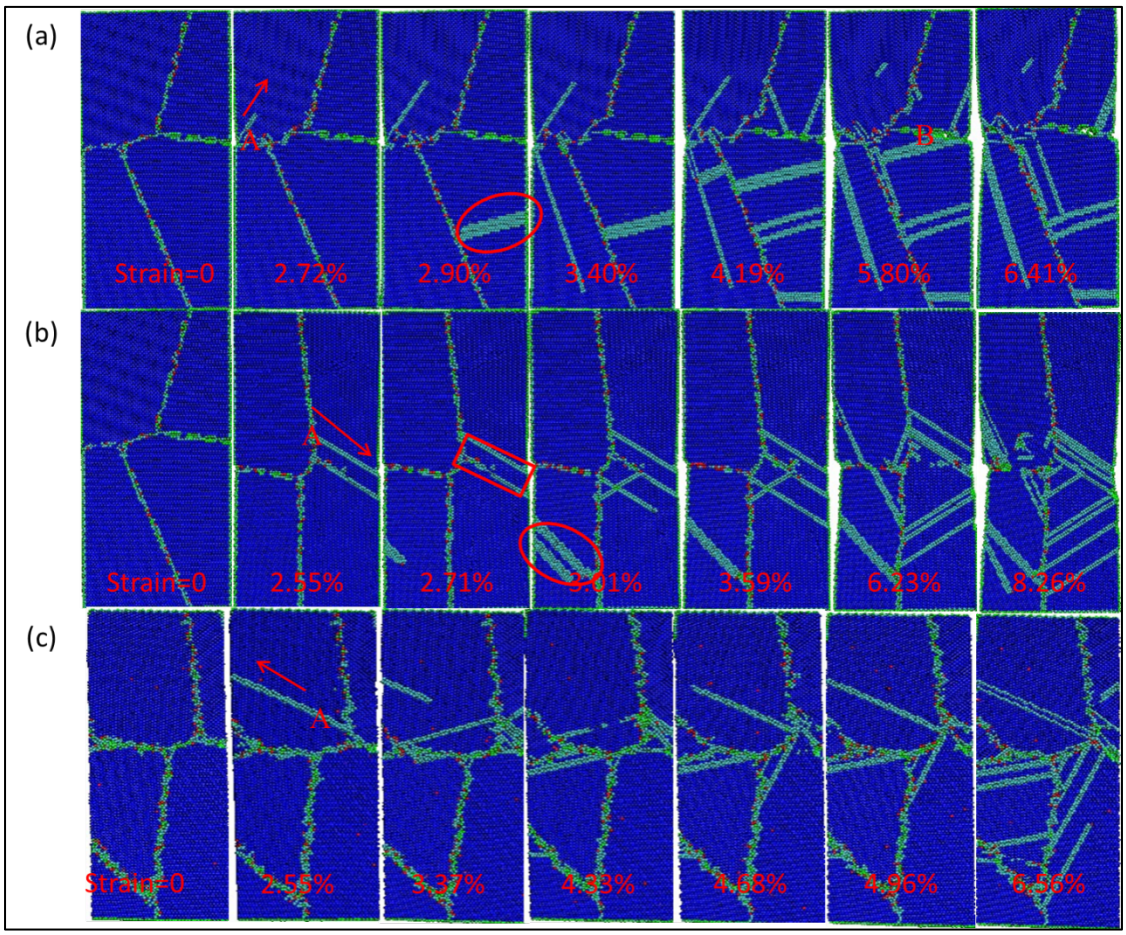
(a)
A
B
Strain=0
2.72%
2.90%
3.40%
4.19%
5.80%
6.41%
(b)
A
B
Strain=0
2.55%
2.71%
3.01%
3.59%
6.23%
8.26%
(c)
A
Strain=0
2.56%
3.37%
4.33%
4.68%
4.96%
6.56%

Figure 7

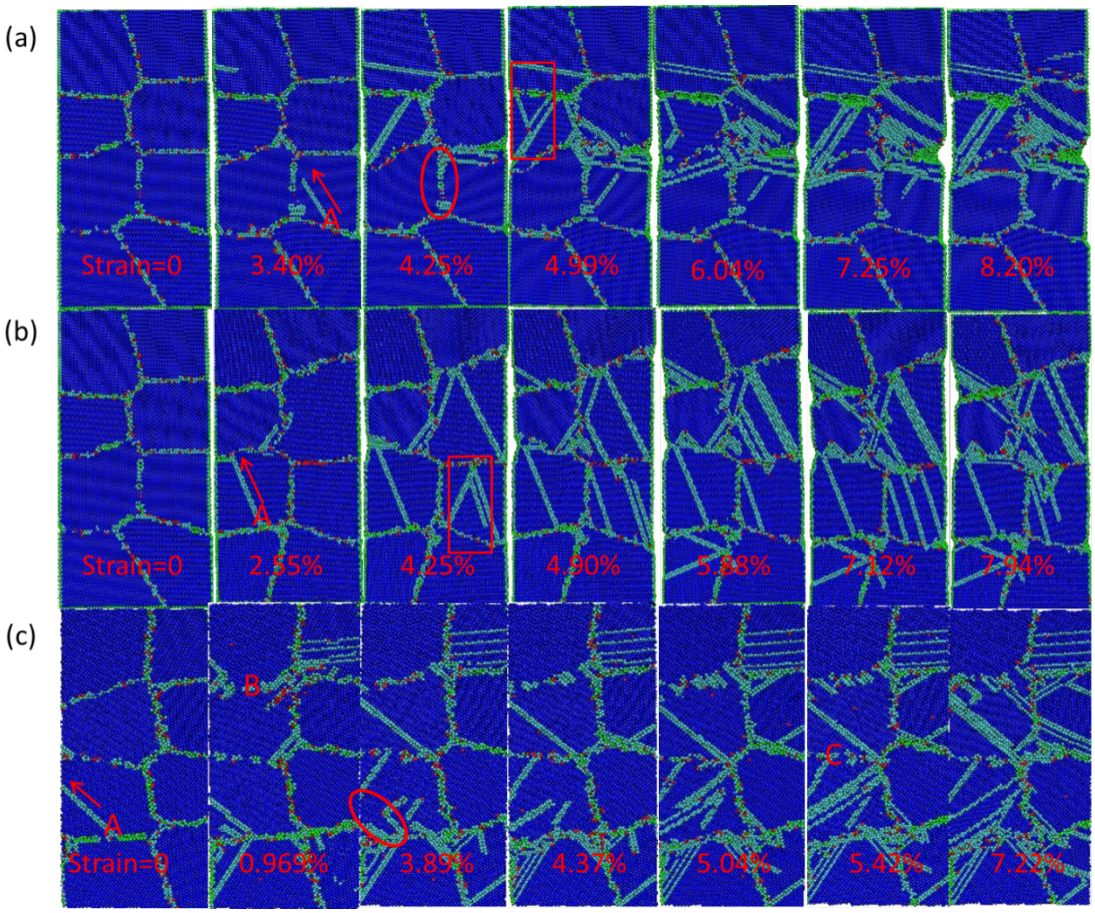
(a)
A
Strain=0
3.40%
4.25%
4.99%
6.04%
7.25%
8.20%
(b)
A
Strain=0
2.55%
4.25%
4.90%
5.88%
7.12%
7.94%
(c)
B
C
A
Strain=0
0.969%
3.89%
4.37%
5.04%
5.42%
7.22%

Figure 8

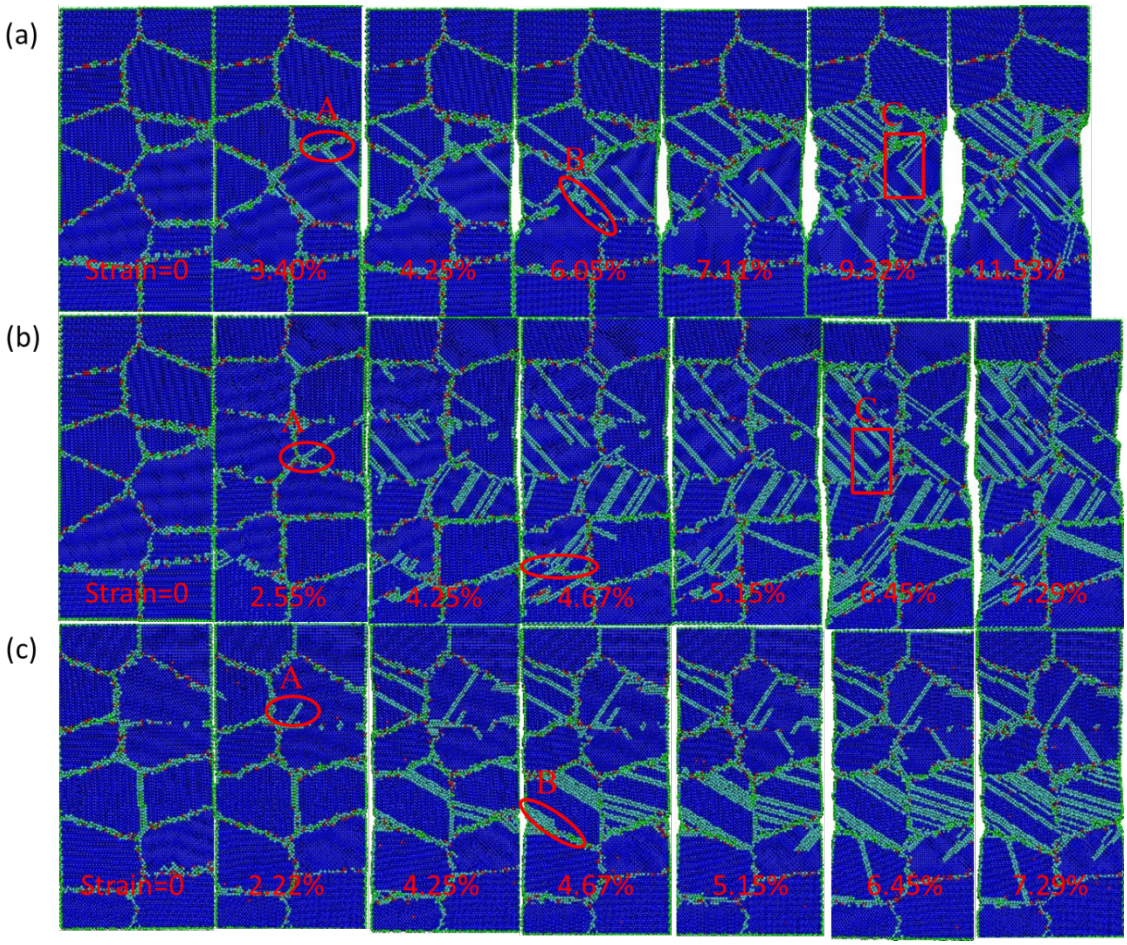
(a)
A
B
C
Strain=0
3.40%
4.25%
6.05%
7.11%
9.32%
11.53%
(b)
A
C
Strain=0
2.55%
4.25%
4.67%
5.15%
6.45%
7.29%
(c)
A
B
Strain=0
2.22%
4.25%
4.67%
5.15%
6.45%
7.29%

Figure 9

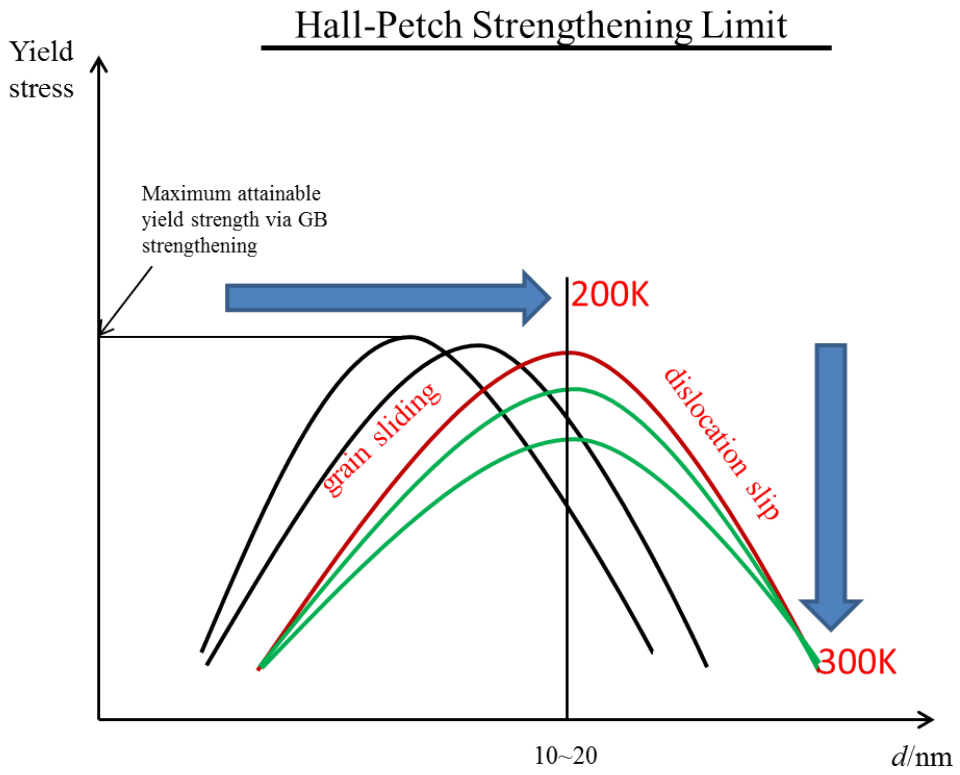
Hall-Petch Strengthening Limit
Yield stress
Maximum attainable yield strength via GB strengthening
200K
grain sliding
dislocation slip
300K
10~20
d/nm